Journal of Materials Science & Technology 84 (2021) 97–104

Contents lists available at ScienceDirect

Journal of Materials Science & Technology

journal homepage: www.jmst.org

Revealing the relationships between alloy structure, composition and plastic deformation in a ternary alloy system by a combinatorial approach

Jianping Lai [a,1], Wen Hu [a,1], Amit Datye [b,*], Jingbei Liu [b], Jan Schroers [b], Udo D. Schwarz [b,c], Jiaxin Yu [a,*]

[a] Key Laboratory of Testing Technology for Manufacturing Process in Ministry of Education, State Key Laboratory of Environment-friendly Energy Materials, Southwest University of Science and Technology, Mianyang 621010, China
[b] Department of Mechanical Engineering and Materials Science, Yale University, New Haven, CT 06511, USA
[c] Department of Chemical and Environmental Engineering, Yale University, New Haven, CT 06511, USA

ARTICLE INFO

Article history:
Received 4 November 2020
Received in revised form
13 December 2020
Accepted 21 December 2020
Available online 30 January 2021

Keywords:
High-throughput
Metallic glass
Plastic deformation
Magnetron co-sputtering
Nanoindentation
Mechanical properties

ABSTRACT

A high-throughput approach based on magnetron co-sputtering of alloy libraries is employed to investigate mechanical properties of crystalline and amorphous alloys in a ternary palladium (Pd)-tungsten (W)-silicon (Si) system with the aim to reveal the difference in plastic deformation response and extract the relevant structure-property relationships of the alloys in the system. It was found that in contrast to crystalline alloys, the amorphous ones, i.e., metallic glasses, exhibited a much smaller fluctuation range in the plasticity parameters (E_r^2/H and W_p/W_t), indicating a significant difference in the plastic deformation mechanism controlling the mechanical properties for the respective alloys. We propose that the inhomogeneous deformation of amorphous alloys localized in thin shear bands is responsible for the weaker compositional dependence of both plasticity parameters, while dislocation gliding in crystalline materials is significantly more dependent on the exact structure, thus resulting in a larger scattering range. Based on the representative efficient cluster packing model, a set of composition-dependent atomic structural models is proposed to figure out the structure-property relationships of amorphous alloys in Pd-W-Si alloy system.

1. Introduction

The plastic deformation of alloys is closely related to their mechanical properties, such as strength and modulus, which are significantly dependent on the alloys' structure [1]. For crystalline alloys, crystal defects, such as dislocations, are the main reason for the lower strength as compared to their theoretical strength, where the dislocation density and mobility essentially determine their plastic deformation response [2]. In contrast to crystalline alloys in which the plastic deformation is carried through dislocation motion [3], amorphous alloys, i.e., metallic glasses, do not contain dislocations, and their plastic deformation initiates via the formation of shear bands [4]. On the atomic scale, the plastic deformation of amorphous alloys originates due to the rearrangement of localized clusters of atoms under an applied shear stress that experience a structural transition by crossing an activation energy barrier [5]. Thereby, the localized clusters of atoms rearranging during deformation are usually referred to as 'shear transformation zone' (STZ) [6]. Different from the dislocation as an inherent defect in crystalline alloys, however, STZs are not intrinsic features of amorphous alloys that are inescapably pre-determined through the material's atomic exact structure, but local motion of atoms and/or groups of atoms characterized by its transience [7].

Nanoindentation testing is an effective experimental method to detect the plastic deformation behavior of materials [8,9] that is able to directly measure the reduced modulus (E_r) and hardness (H) of a material. Furthermore, the irreversible or plastic work (energy) (W_p) can be obtained by calculating the difference between the area under the loading curve, reflecting the total mechanical work done during an indentation cycle (W_t), and the unloading curve (the elastic work) (W_e). Based on the above mechanical parameters, both

* Corresponding authors.
E-mail addresses: amit.datye@yale.edu (A. Datye), yujiaxin@swust.edu.cn (J. Yu).
[1] Jianping Lai and Wen Hu contributed equally to this work.

https://doi.org/10.1016/j.jmst.2020.12.038
1005-0302/

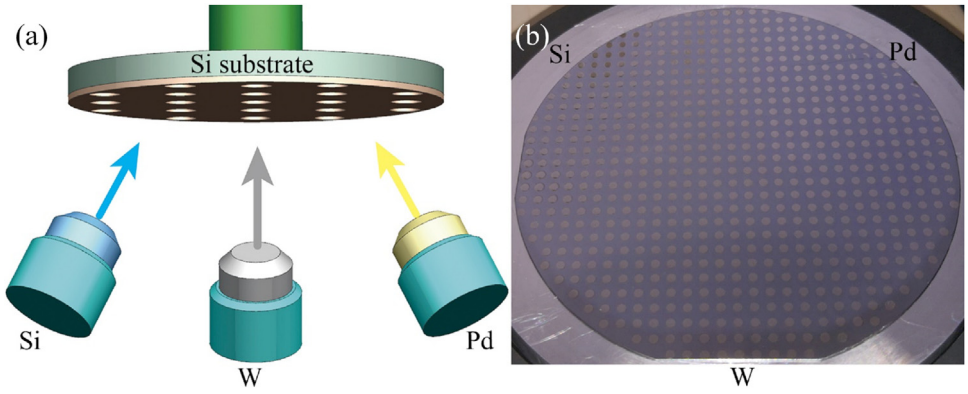

Fig. 1. (a) Schematic illustration of the magnetron setup for the co-sputtering of the Pd-W-Si alloy library; (b) The appearance of the fabricated thin-film Pd-W-Si alloy library on the silicon substrate, in which there are 672 patches of ≈3 mm in diameter, with each patch containing one individual alloy composition.

the reduced modulus^2/hardness ratio E_r^2/H [10,11] and the energy dissipation ratio W_p/W_t [12–14] have been used to assess the plastic deformation ability of materials. Experimental investigation on five materials having a wide range of plasticity showed that the energy dissipation ratio (W_p/W_t) was higher in materials with a larger plasticity [11]. E_r^2/H is proportional to P_m/h_s^2, where P_m is the applied peak load and h_s is the elastic surface displacement at the perimeter of contact [11]. Since h_s represents the capability of elastic recovery of materials during indentation, the E_r^2/H ratio having the reciprocal relationship with h_s can be thought to be an indicator of the plastic deformation ability. In other words, the higher the E_r^2/H ratio, the greater the plasticity of the materials is. As a result, both E_r^2/H and W_p/W_t are practical engineering parameters to evaluate the plastic deformation of crystalline alloys. Due to the significant difference in the structure and deformation mechanisms of crystalline and amorphous alloys [5,15], it is interesting to see how these 'plasticity parameters' E_r^2/H and W_p/W_t behave in alloy systems that are similar in composition, but differ in their degree of long-range order.

The magnetron co-sputtering approach allows different elements to be co-deposited from separate sources onto a substrate, resulting in a compositionally graded film on the substrate [16–19]. Further analysis of local areas using electron spectroscopy, x-ray diffraction, and nanoindentation then results in the availability of data covering several hundreds of alloy compositions at once. Previous studies have successfully developed high-throughput approaches in exploring new amorphous alloys with desired physical properties [19–21]. For example, Ding et al. used a high-throughput approach based on parallel blow forming to identify the proper alloy compositions with the highest thermoplastic formability in the magnesium (Mg)-copper (Cu)-yttrium (Y) ternary alloy system [20]. Li et al. employed a high-throughput strategy to rapidly identify the composition range with a high glass forming ability (GFA) in the Ir-Ta-Ni system [21]. However, only a few studies have focused on establishing the dependence of alloy composition on the mechanical properties using high-throughput methods. Using the magnetron co-sputtering approach, Schnabel et al. fabricated the combinatorial Co-Zr-Ta-B metallic glass thin films with a continuous concentration gradient, and systematically revealed the relationships between chemical composition and mechanical properties of metallic glasses [22]. Recently, we studied the mechanical properties of Mg-Zn-Ca and Mg-Zn-Fe ternary systems that revealed the optimal alloy compositions suitable for biomedical applications [19]. Since most alloy samples prepared in the Mg-Zn-Ca and Mg-Zn-Fe systems were nearly fully amorphous with no crystalline counterparts, the comparison of mechanical properties between amorphous and crystalline alloys in a same alloy library could not be made. Therefore, more attempts deserve to be made to explore the intrinsic difference of mechanical behavior by comparing the plastic deformation response of crystalline and amorphous alloys within a same alloy system.

In this work, a Pd-W-Si ternary library consisting of both crystalline and amorphous structures was deposited on a silicon wafer using magnetron co-sputtering. Nanoindentation was used to analyze over 600 different local compositions for their mechanical properties. The plastic deformation response of crystalline and amorphous alloys within this alloy system was then investigated by comparing the plasticity parameters of E_r^2/H and W_p/W_t and the intrinsic relationship between plastic deformation and alloy's structure was properly established. In addition, based on the relationship between the composition of an amorphous alloy and its elastic modulus, atomic packing models were discussed.

2. Material and methods

2.1. Preparation of the Pd-W-Si library

The thin film wafer of the Pd-W-Si library was produced by direct current (DC) magnetron co-sputtering (AJA International ATC 2200) onto a silicon substrate. The silicon substrates were purchased from WRS Materials (San Jose, CA). The three sputtering targets were arranged at an angle of 120 degrees with each other around the substrate (Fig. 1(a)). The sputtering targets were tilted by 19° towards the normal axis of the substrate. The orientation angles of the sputtering guns relative to the substrate and the sputtering power applied were manipulated to control the fabrication of compositionally graded films. The elemental targets with a purity of 99.95 % for Pd and W and 99.5 % for Si were purchased from Kurt Lesker Company. The Pd-Si binary system was first selected because of its excellent glass-forming ability (GFA) [23,24]. Since W has a high Young's modulus (411 GPa) [25], the incorporation of W into Pd-Si binary system is expected to enhance the mechanical properties of alloys in ternary system, based on the "rule of mixture" [26]. The detailed parameters of sputtering were a power of 89 W for Pd, 50 W for W, and 50 W for Si. The Pd-W-Si library was deposited on a silicon substrate with a diameter of 100 mm and a thickness of 550 μm. A mask was applied during sputtering and a library of ≈3 mm diameter circular patches on a square grid with 6 mm center-to-center spacing was fabricated, as shown in Fig. 1(b). There were 672 patches on the wafer, and each patch contained one individual alloy composition. The thickness of each individual Pd-W-Si combinatorial library patch was approximately 1 μm with a thickness variation of less than 20 % from center of the wafer to its edge. Using the white-light scanning profilometer (Rtec, USA), the root-mean-square (RMS) roughness of the alloy patch was quanti-

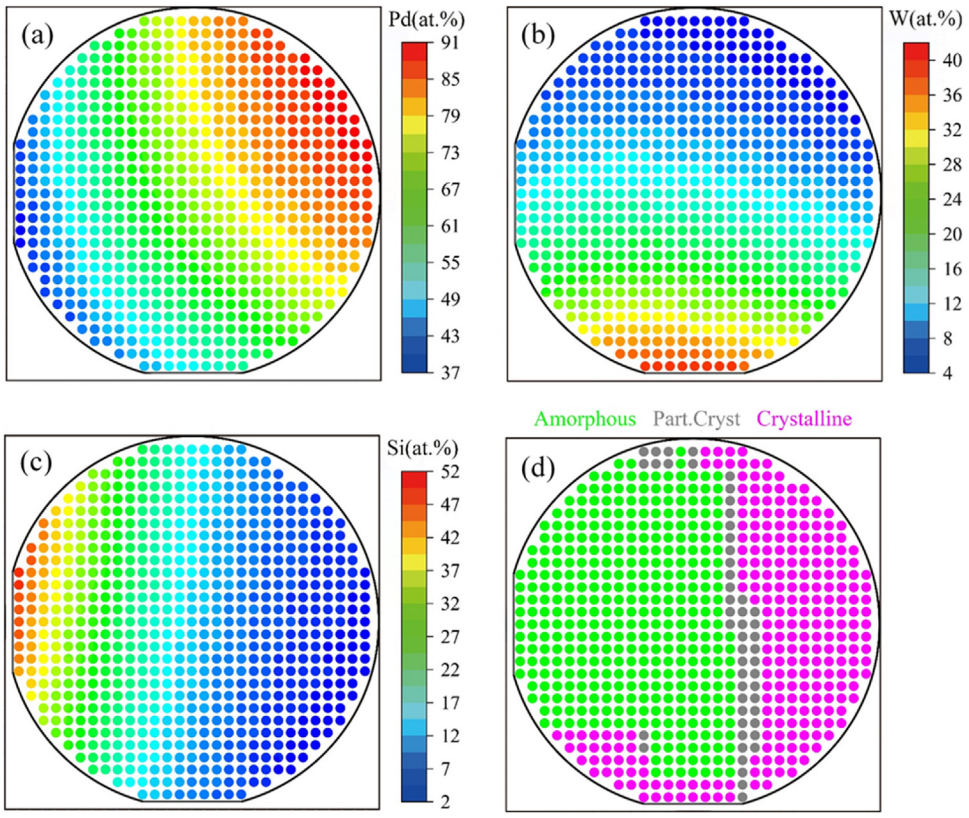

Fig. 2. The compositional distribution of (a) Pd, (b) W, and (c) Si across the sputtered wafer, as measured by EDX; (d) XRD analysis of the combinatorially sputtered wafer exposing the phase of each patch.

fied as ~1.5 nm for an area of 200 μm × 200 μm, which was the average value of at least individual 50 patches within the wafer.

2.2. Structural, compositional, and mechanical properties characterization of the Pd-W-Si library

X-Ray diffraction (XRD) was performed using a Rigaku SmartLab X-ray diffractometer with Cu$K\alpha$ radiation to determine the structure of each patch on the film. Similarly, energy dispersive X-ray spectroscopy (EDX) analysis was carried out using an Oxford Instruments X-Max detector attached to a Zeiss Sigma VP field emission scanning electron microscope at the center of each patch to determine the alloy composition.

The reduced modulus (E_r) and the hardness (H) of each library patch was characterized using a nanoindenter (G200, Keysight, USA) with a diamond Berkovich indenter tip. The Berkovich indenter was purchased from Micro Star Tech with a radius of 20 nm and then calibrated by indentations using standard fused silica before standard testing. When the thermal drift reached 0.1 nm/s, the indenter was slowly driven toward the surface at a constant displacement rate of 10 nm/s until surface contact was detected by the changes in the load and displacement signals. After contact, a permanent hardness impression was made by driving the indenter into the specimen to a depth of 100 nm to avoid substrate effects [27–29], where the strain rate was set as constant 0.05/s and holding time was 2 s. At the end of the unloading, the indenter was held on the surface for 100 s to establish the rate of thermal drift in the machine and specimen for correction of the data, and then completely withdrawn. E_r and H can then be directly evaluated through the analysis of the accurate load-displacement data obtained [8,9,30]. It should be mentioned that the E_r and H derived here did not consider any pile-up or sink-in effect. In addition, the plastic energy W_p, representing the mechanical work done by plastic deformation, can be extracted by determining the area between loading and unloading curves, while the total dissipated energy W_t can be calculated from the area under the loading curve, reflecting the total mechanical work done by the indenter [12–14].

3. Results

Fig. 2 depicts the compositional distributions and corresponding structure of the individual patches in the Pd-W-Si library. First, the species-specific compositions of the patches are displayed in Fig. 2(a–c), revealing continuous compositional gradients of the alloy's constituents ranging from 39–90 at.% for Pd, 5–40 at.% for W, and 3–49 at.% for Si, respectively. In addition, XRD measurement was performed to identify the structure of each alloy patch on the wafer, the results of which are shown in Fig. 2(d). It was found that, depending on the local alloy composition, the patches were either fully amorphous (green), fully crystalline (pink), or, in a narrow transitional area marked with grey, partially crystalline with an amorphous matrix. By comparing the compositional evolution of Pd, W, and Si elements with the phase distribution on the wafer, the Si exhibited a stronger dependence on the phase structure than other two elements, which manifested in the similar orientation of the boundary distinguishing the amorphous and crystalline alloys with the equal-composition lines for Si (Fig. 2(c) and (d)). This may be associated with an ability of Si in inhibiting crystallization of supercooled liquid due to their desire to form oriented bonds [31].

To distinguish the effect of local alloy compositions in the Pd-W-Si library on the reduced modulus E_r and hardness H clearly, E_r and H are plotted against the variations of alloy composition as ternary diagrams in Fig. 3(a) and (b). Depending on the variations of alloy composition, E_r and H covered a wide range between 20.8–162.6 GPa and 4.0–8.7 GPa, respectively. The plasticity parameters E_r^2/H (Fig. 3(c)) and W_p/W_t (Fig. 3(d)) were then calculated to unveil

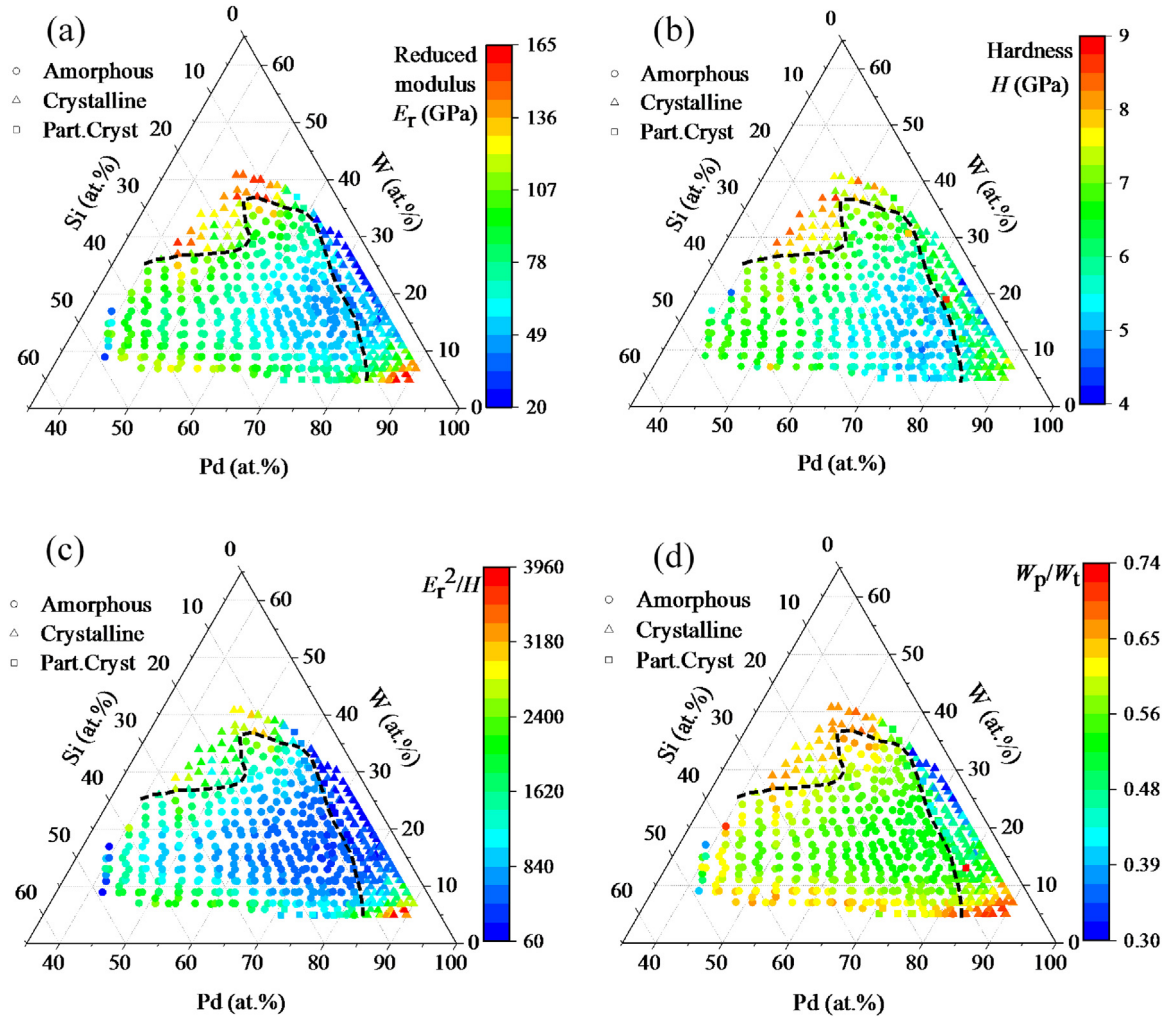

Fig. 3. The dependence of (a) E_r, (b) H, (c) E_r^2/H, and (d) W_p/W_t on the elemental composition of Pd-W-Si alloys, respectively. The dotted lines mark the boundary between amorphous and crystalline patches.

the plastic deformation response of the amorphous and crystalline alloys. We found that both E_r^2/H and W_p/W_t varied as a function of alloy composition with a distribution range of 71.0–3947 and 0.30–0.74, respectively. The alloy compositions are similar for extreme values in the parameters, which are identified to be Pd_{70}-W_{27}-Si_3 and Pd_{88}-W_5-Si_7 at the minimum and maximum value of E_r^2/H and Pd_{70}-W_{27}-Si_3 and Pd_{84}-W_5-Si_{11} at the minimum and maximum value of W_p/W_t, respectively.

4. Discussion

4.1. Comparison of plastic deformation response for amorphous and crystalline alloys

Based on the data presented in the Results section, it is intriguing to see how the parameters of E_r^2/H and W_p/W_t, which are thought to track the material's plastic deformation response, behave in amorphous and crystalline alloys. Fig. 4 shows a comparison of E_r^2/H and W_p/W_t as a function of Pd and Si contents for the respective amorphous and crystalline alloys in the Pd-W-Si system. Both E_r^2/H and W_p/W_t display a different extent of dependence on alloy composition for crystalline and amorphous alloys. For example, E_r^2/H fluctuates between 369 and 2597 for amorphous alloys, but for crystalline alloys, it covers a much wider range of 71–3947 despite comprising similar chemical compositions. Similarly, W_p/W_t varies in a range of 0.503–0.682 for amorphous alloys and 0.305–0.731 for crystalline alloys. Obviously, compared to crystalline alloys, the amorphous alloys exhibit a much weaker compositional dependence in both parameters of E_r^2/H and W_p/W_t, which reveals that the crystalline and amorphous alloys undergo a different plastic deformation response.

This remarkable difference in the plastic deformation response can be concluded as being clearly related to the origins of plastic deformation in the two kinds of alloys. For crystalline alloys, dislocations are the basic carriers of plastic deformation. Under a certain stress condition, dislocations proliferate as needed and migrate along glide planes, which enables the plastic strain to be accommodated by the entire stressed volume. Due to the migrating character of dislocations, the plastic deformation is carried continuously, and each volume of crystalline samples that is exposed to stress above a certain material-dependent threshold contributes to their plastic deformation. In contrast, for amorphous alloys, STZs are the basic carriers of plastic deformation, as discussed in the introduction. Different from dislocations, the mobility of STZs is very poor, meaning STZs can be considered to be essentially immobile [7]. When the applied stress increases beyond a critical point, many STZs will self-organize and gradually develop into mature shear bands. The shear bands then enable relative sliding of the material, analogous to the crack propagation in their crystalline counterparts, and may eventually lead to macroscopic fracture. Due

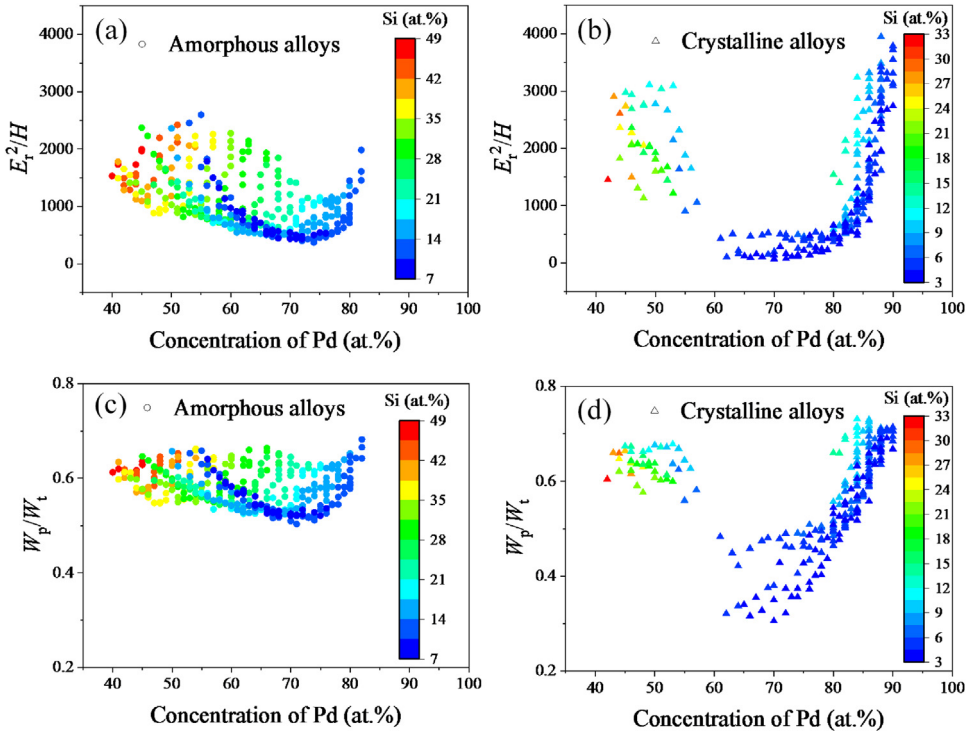

Fig. 4. The 'plasticity parameters' E_r^2/H (a, b) and W_p/W_t (c, d) plotted as a function of Pd and Si concentrations in amorphous and crystalline patches of the Pd-W-Si alloy library, respectively.

to the immobile character of shear bands, the plastic deformation of amorphous alloys is highly localized in the such thin shear bands [1]. As a consequence, lesser volume in the sample is activated to participate in the accommodation of plastic strain if compared to crystalline materials, explaining why crystalline alloys exhibit a higher plasticity than their amorphous counterparts.

For amorphous alloy, previous studies have suggested that there is a correlation between the volume shear bands occupy in the material and alloy's plasticity [32,33], i.e., an amorphous alloy with a larger shear band volume tends to have a better plasticity. For crystalline counterparts, the plasticity is strongly dependent on the type of crystal structure established, as this determines the quantity of dislocation glide systems accessible and the energy barrier inhibiting dislocation gliding. For example, crystalline materials with the faced-centered-cubic (FCC) structure generally show a greater plasticity than materials with body-centered-cubic (BCC) and hexagonal close-packed (HCP) structures due to the availability of more dislocation glide systems [34]. For the Pd-Si system, the crystal structure was identified to be FCC for single-crystalline Pd, orthorhombic for Pd_9Si_2 and Pd_3Si, and hexagonal for Pd_2Si, respectively [35–37]. From Fig. 4(b) and (d), we see that with the increase of Pd content from ~65 to ~90 at.%, both E_r^2/H and W_p/W_t increased monotonically, which might be explained by the transition of crystal structure from HCP to FCC.

As discussed above, both an amorphous material's shear band volumes and a crystalline material's structure-dependent ability to accommodate plastic flow through glide planes are highly dependent on alloy's composition, but the degree to which these two factors contribute to the plasticity is remarkably different. As compared to amorphous alloys, the energy barrier that needs to be overcome to initiate plastic flow along a certain glide plane will be remarkably different for crystalline alloys with various compositions, which is expected to exert a significant effect on the plastic deformation response of the alloys. Therefore, the parameters E_r^2/H and W_p/W_t, reflecting the plastic deformation response, show a much weaker compositional dependence (smaller fluctuation range) for amorphous alloys than the crystalline alloys in the same ternary alloy system.

By using this high-throughput technique, the effect of chemical composition on a material's plastic deformation response can be continuously tracked for amorphous and crystalline alloys in the same system, thereby establishing a database covering several hundreds of samples. Even though many previous efforts were made to figure out the difference of deformation mechanism in a statistical manner [25,38], the reliability of the results was often limited due to the low number of samples and different origins of the assembled experimental data. Overcoming these limitations, the present work establishes a higher confidence level due to the large quantity of samples fabricated under essentially identical processing conditions.

4.2. The relationship between atomic structure and mechanical properties in amorphous alloys

In Fig. 5(a), we chart the reduced modulus E_r as a function of the concentration of Pd and Si for the 363 amorphous Pd-W-Si alloys. It was found that, with increase in the concentration of Pd, E_r decreased statistically. To gain an even different perspective, we then extracted from the E_r values as a function of the concentration of W and Pd, which is plotted in Fig. 5(b). For the amorphous alloys with identical concentration of Pd, E_r first decreases with increasing W before it gradually increases again. It is well known that in an amorphous alloy system the modulus is closely related to the constituent elements and their atomic bonds, which are significantly dependent on the alloy composition [39–41]. However, the details of how the constituent elements that are related to the exact atomic structures and atomic bonds affect the properties of the alloys is not exactly explored, which is useful to bridge the structure-property relationship in amorphous alloys. The following section will explore how the atomic structure, which naturally depends on the alloy composition, affects the modulus of amorphous alloys.

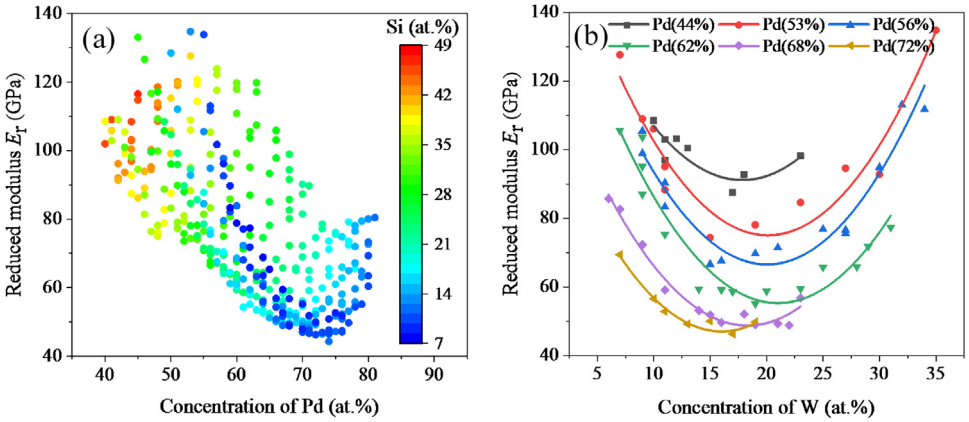

Fig. 5. (a) The reduced elastic modulus E_r as a function of the Pd and Si concentrations for the 363 amorphous Pd-W-Si alloys; (b) E_r plotted as a function of the concentrations of W and Pd as extracted from the data in (a).

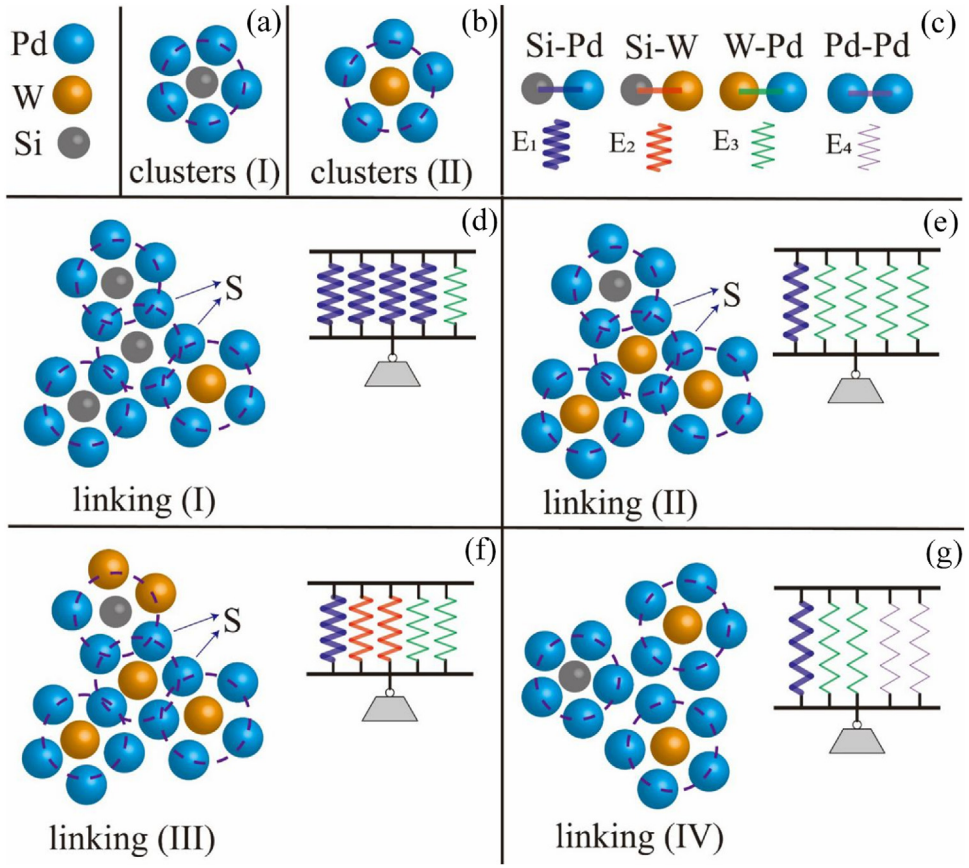

Fig. 6. The proposed atomic model in the ternary Pd-W-Si amorphous alloys: (a) clusters (I) and (b) clusters (II) represent the Si-centered clusters and W-centered clusters in the system respectively; (c) The springs of E_1, E_2, E_3, and E_4 represent the bonding strength of Si-Pd, W-Pd, Si-W, and Pd-Pd, respectively; (d) linking (I) and (e) (II) represent predominantly Si-centered clusters and W-centered clusters with a low and medium concentration of W, respectively; (f) linking (III) reflects clusters with a relatively high concentration of W; (g) linking (IV) illustrates a situation where type (I) and type (II) clusters are adhering by solvent-solvent (Pd-Pd) bonding in materials with a high concentration of Pd. The letter "S" in (d), (e), and (f) denotes shell Pd atoms, and the purple dashed circles delineate the clusters.

Due to the complexity of the atomic structure in an amorphous alloy, it is extremely difficult to characterize their definite structure by experimental techniques, and thus a variety of theoretical atomic structural models have been proposed to elucidate the structure-property relationships in amorphous alloys [42,43]. Among these models, the efficiently packing model (ECP) [44] is found to exhibit some predominance in describing solute-solvent amorphous alloys. Based on this model, schematic structural arrangements of the atomic constituents in various compositions of the Pd-W-Si alloy system are proposed in Fig. 6. The compositional range of amorphous alloys is 39–82 at.% for Pd, 5–35 at.% for W, and 8–49 at.% for Si, respectively. In most cases, Pd has a much higher concentration than other two elements and therefore considered to be the solvent atoms, while Si and W can be considered as solute atoms. Due to the rule of the solute-solute avoidance [45], two basic atomic clusters are proposed, as shown in Fig. 6(a) and (b), where Si and W are the center solute atoms that are surrounded by solvent Pd atoms. With the variation of Pd, Si, and W concentrations

in the system, the way how the two basic clusters are linked varies, which naturally influences the alloy's mechanical properties, such as Young's modulus.

Previous investigations proposed some rules between amorphous alloys' elements and their Young's moduli, such as the "rule of inheritance" [39,46] and the "rule of mixture" [26,47]. For rationalizing the rule of inheritance, it was considered that the moduli of amorphous alloys inherited the individual moduli from their constituent base elements (that is, their solvent components). However, since the rule of inheritance mainly considered the contribution of solvent elements on the alloys' Young's modulus, the effect of specific concentrations of each element and their corresponding preferred atomic clusters cannot be clarified. The "original" rule of mixture, proposed by Wang et al. [26], therefore suggested that the predicted Young's modulus of an amorphous alloy was equal to the weighted average of the elastic moduli for the constituent elements. Since the original rule of mixture does not consider the contributions of atomic clusters and related "effective atomic bond strength" to the alloys' modulus, it also presents some limitations to understand the relationship between an alloys' composition and its Young's modulus.

To alleviate some of the original rule of mixture's shortcomings, a "new rule of mixture" proposed by Zhao et al. considered weighted average on the Young's modulus of constituent atomic bonds [40,41], that is, $M = \sum f_i M_i$, where M represents Young's modulus of amorphous alloys, f_i is the atomic fraction of the ith atomic bonds, and M_i is modulus of the ith atomic bonds. This theory considered the contribution of individual atomic bonds to the modulus of alloys, which was ignored in the assumptions that led to the creation of the "original" rule of mixture [26]. The theory predicted Young's moduli that were satisfactorily close to the experimentally obtained values for many systems, in particular for systems where the original rule of mixture did not deliver good matches [41]. For example, according to the original rule of mixture using atoms as constituent components, the modulus of amorphous alloys with a fixed Pd content should increase with increasing W due to the fact that its modulus of 411 GPa is the highest among the three elements. However, we see from Fig. 5(b) that the modulus of amorphous alloys decreases monotonously with W increasing from ~5 % to 15 %, in obvious contradiction to the expectations of the "original" rule of mixture. The amorphous alloys with increasing W content do not benefit from tungsten's high modulus, suggesting that the rule of mixture does not work in this case. In fact, the increase of tungsten concentration actually raises the proportion of Pd-W bonds in the system and decreases the Pd-Si bonds simultaneously. Therefore, according to the "new rule of mixture", the variation of atomic bonds should be the main reason affecting the alloy modulus rather than the variation of atoms quantity. Based on these assumptions, the Young's modulus of amorphous alloys in ternary Pd-W-Si system can be expressed as Eq. (1):

$$E = \chi_{\text{Pd-Si}} \times E_{\text{Pd-Si}} + \chi_{\text{Pd-W}} \times E_{\text{Pd-W}} + \chi_{\text{W-Si}} \times E_{\text{W-Si}} + \chi_{\text{Pd-Pd}} \times E_{\text{Pd-Pd}} + \chi_{\text{W-W}} \times E_{\text{W-W}} + \chi_{\text{Si-Si}} \times E_{\text{Si-Si}} \quad (1)$$

where $\chi_{\text{A-B}}$ and $E_{\text{A-B}}$ are the fraction of A-B bonds out of all bonds in the material and the Young's modulus of a material only featuring A-B bond [40,41], respectively. A and B represent any two elements in the ternary system. Considering the rule of the solute-solute avoidance [45], the W-W and Si-Si bonds are expected to be very few in the system. Thus, the Young's modulus of amorphous alloys in Pd-W-Si system are mainly determined by other four atomic bonds, as showed by the following Eq. (2):

$$E = \chi_{\text{Pd-Si}} \times E_{\text{Pd-Si}} + \chi_{\text{Pd-W}} \times E_{\text{Pd-W}} + \chi_{\text{W-Si}} \times E_{\text{W-Si}} + \chi_{\text{Pd-Pd}} \times E_{\text{Pd-Pd}} \quad (2)$$

The bonding strength between different elements was reported to be larger than that between same elements [39,41], indicating the weaker bonding strength of Pd-Pd bonds than other three atomic bonds with different elements. Consequently, the modulus of amorphous alloys in Pd-W-Si system is presumed to be largely governed by the proportions of Pd-Si, W-Pd, and Si-W bonds present in the material compared to the total number of bonds. It was reported that the atomic bonding strength of atomic pairs in amorphous alloys was closely related to its mixing enthalpy and the atomic bonding strength increased with the absolute value of mixing enthalpy [39]. In the Pd-W-Si alloy system, the mixing enthalpy of Pd-Si atomic pair was calculated to be −55 kJ/mol, much higher than that of Pd-W (−6 kJ/mol) and Si-W (−31 kJ/mol) atomic pairs [39,40]. As a result, the bonding strength of different atomic bonds in Pd-W-Si system is sequenced as below: Si-Pd > Si-W > W-Pd > Pd-Pd, which are schematically shown in Fig. 6(c) using various springs.

In the Pd-W-Si amorphous alloy system, for a fixed Pd concentration from 44 to 72 at.%, when W concentration is low, the system can be considered as an Si-rich system, where more Si-centered clusters (cluster I) and less W-centered clusters (cluster II) are linked by sharing Pd (solvent) atoms in the shell according to the ECP model, as shown in Fig. 6(d). Due to the more Si-centered clusters, according to Eq. (2), the value of $\chi_{\text{Si-Pd}}$ in the system is relatively high and consequently, the modulus of alloys is controlled largely by the Si-Pd bonds. The bonding strength of Si-Pd is the strongest among constituent atomic bonds in the system due to its largest mixing enthalpy, contributing the high modulus of amorphous alloys with a low W concentration. With the increase in W, the centered Si atoms have to decrease and be substituted by the W atoms, thus leading to more linking II, as shown in Fig. 6(e), where more W-centered clusters (cluster II) and less Si-centered clusters (cluster I) are linked by sharing Pd atoms. In other words, with increasing W content, $\chi_{\text{Si-Pd}}$ in the system decreases inevitably and $\chi_{\text{W-Pd}}$ increases progressively. Here, because of the more W-centered clusters, the modulus of alloys is more determined by the bond strength of W-Pd. Due to the low bonding strength of W-Pd, the modulus of Pd-W-Si amorphous alloys will reduce. While the W content further increase, the W atoms will replace the solvent Pd atoms due to their close atomic radius, and Si atoms will escape into the interspaces between the solvent atoms due to the smallest atomic radius and still act as the solute atoms, as shown in the Linking III in Fig. 6(f). In this situation, due to more Si-W bonds in the system, the high bonding strength causes the modulus to increase again. Therefore, as the W increases from 5 to 35 at.% in Fig. 5(b), for each fixed Pd concentration, the predominant atomic bonds in the linking model evolve from the strong Pd-Si to weak Pd-W and to strong W-Si atomic pairs. As a result, for each fixed concentration of Pd, E_r shows a trend that the modulus of amorphous alloys decreases first and then increases with further increasing W content.

Another phenomenon that should be noted is the fact that the modulus of Pd-W-Si amorphous alloys decreases with increasing Pd content, independent on the concentration of W and Si (see Fig. 5(a) and (b)). Previous investigations revealed that the deformation of amorphous alloys mainly occurred at the compliant solvent-solvent junctions due to their weak bonding strength [39,46]. When the solvent Pd atoms increase, the linking way among clusters is preferable to evolve from solute-solvent linking by sharing shell atoms into solvent-solvent linking without sharing shell atoms, as shown in Fig. 6(g). Based on the above analysis, the progressive decrease of E_r with increasing Pd content is well understood with a change of the atomic linking model from the strong solute-solvent way (Pd-Si/Pd-W/W-Si) to weak solvent-solvent linking way (Pd-Pd) (Fig. 6(d, e, f→g)).

The deformation mechanism of amorphous alloys is one of the most challenging issues in the field, which has not been comprehensively understood due to their complicated structure. In this work, the compositional dependence of plasticity parameters in amorphous and crystalline systems is rationalized by comparing the intrinsic difference between forming shear banding and dislocation slip, which advances a deeper understanding of the factors governing mechanical properties (e.g., strength and plasticity) and the related structure-property relationships for amorphous alloys. In addition, it appears possible to design, at least approximately, an amorphous alloy composition with enhanced mechanical properties based on relevant empirical criteria. For example, the yield strength (σ_y) can be estimated via the hardness of alloys (H) ($H \approx 2.9\sigma_y$), and the plasticity parameters of ${E_r}^2/H$ and W_p/W_t can assist in evaluating the plastic deformation ability of ternary alloys. As a consequence, the specific alloys with high strength and simultaneous plasticity can be selected from a certain ternary alloys system.

5. Conclusions

In this work, a Pd-W-Si ternary alloy library featuring both crystalline and amorphous structures was fabricated using magnetron co-sputtering and subsequently examined by nanoindentation. With the power of a high-throughput approach leading to a statistically solid data base, a comparison of plastic deformation response of crystalline and amorphous alloys is made and elaborated, and the structural evolution with varying alloy's composition in amorphous system is revealed. The detailed conclusions are drawn as below:

(1) Compared to their crystalline counterparts, the amorphous alloys in the Pd-W-Si system exhibited a much weaker compositional dependence in the plasticity parameters of ${E_r}^2/H$ and W_p/W_t, which can be rationalized by considering the different deformation mechanisms controlling the plastic deformation response of crystalline and amorphous alloys. More specifically, this finding is ascribed to the lower ability of accommodating plastic strain for amorphous alloys through shear band formation than the crystalline alloys by dislocation glide.
(2) The modulus of amorphous alloys exhibited a parabolic shape with increasing W content. Based on the "new rule of mixture", a set of atomic structural models is proposed dependent on alloy composition to explain the observed structure-property relationships, which are found to satisfactorily describing the variations in the modulus of amorphous alloys.

Declaration of Competing Interest

The authors report no known competing interests.

Acknowledgements

This work was financially supported by the National Natural Science Foundation of China (No. 51975492), the Research Fund Supported by Sichuan Science and Technology Program (No. 2018JY0245), and the Natural Science Foundation of Southwest University of Science and Technology (No. 19xz7163). Work by A. Datye and U.D. Schwarz was supported by the National Science Foundation of the United States (No. NSF CMMI-1901959).

References

[1] M.M. Trexler, N.N. Thadhani, Prog. Mater. Sci. 55 (2010) 759–839.
[2] A. Stukowski, K. Albe, Model. Simul. Mater. Sci. 18 (2010) 2131–2145.
[3] X. Jiang, J.J. Zhao, X. Jiang, Comput. Mater. Sci. 50 (2011) 2287–2290.
[4] J.X. Li, G.B. Shan, J.X. Li, G.B. Shan, K.W. Gao, L.J. Qiao, W.Y. Chu, Mater. Sci. Eng. A 354 (2003) 337–343.
[5] C.A. Schuh, T.C. Hufnagel, U. Ramamurty, Acta Mater. 55 (2007) 4067–4109.
[6] A.S. Argon, Acta Metall. 27 (1979) 47–58.
[7] A.L. Greer, Y.Q. Cheng, E. Ma, Mater. Sci. Eng. R 74 (2013) 71–132.
[8] W.C. Oliver, G.M. Pharr, J. Mater. Res. 7 (1992) 1564–1583.
[9] G.M. Pharr, W.C. Oliver, F.R. Brotzen, J. Mater. Res. 7 (1992) 613–617.
[10] W.C. Oliver, G.M. Pharr, J. Mater. Res. 19 (2004) 3–20.
[11] Y.W. Bao, W. Wang, Y.C. Zhou, Acta Mater. 52 (2004) 5397–5404.
[12] A. Datye, H.T. Lin, Ceram. Int. 43 (2017) 800–809.
[13] Y.T. Cheng, C.M. Cheng, Appl. Phys. Lett. 73 (1998) 614–616.
[14] Y.T. Cheng, C.M. Cheng, Mater. Sci. Eng. R 44 (2004) 91–149.
[15] J. Eckert, J. Das, S. Pauly, C. Duhamel, J. Mater. Res. 22 (2007) 285–301.
[16] Y.H. Liu, Z.H. Hu, Z.G. Suo, L.Z. Hu, L.Y. Feng, X.Q. Gong, Y. Liu, J.C. Zhang, Sci. China Technol. Sci. 62 (2019) 521–545.
[17] S.A. Kube, W.T. Xing, A. Kalidindi, S. Sohn, A. Datye, D. Amram, C.A. Schuh, J. Schroers, Acta Mater. 188 (2020) 40–48.
[18] S.A. Kube, S. Sohn, D. Uhl, A. Datye, A. Mehta, J. Schroers, Acta Mater. 166 (2019) 677–686.
[19] A. Datye, S.A. Kube, D. Verma, J. Schroers, U.D. Schwarz, J. Mater. Chem. B 7 (2019) 5392–5400.
[20] S.Y. Ding, Y.H. Liu, Y.L. Li, Z. Liu, S. Sohn, F.J. Walker, J. Schroers, Nat. Mater. 13 (2014) 494–500.
[21] M.X. Li, S.F. Zhao, Z. Lu, A. Hirata, P. Wen, H.Y. Bai, M.W. Chen, J. Schroers, Y.H. Liu, W.H. Wang, Nature 569 (2019) 99–103.
[22] V. Schnabel, M. KöHler, S. Evertz, J. Gamcova, J. Bednarcik, D. Music, D. Raabe, J.M. Schneider, Acta Mater. 107 (2016) 213–219.
[23] K.F. Yao, N. Chen, Sci. China Ser. G-Phys. Mech. Astron. 4 (2008) 414–420.
[24] N. Chen, K.F. Yao, F. Ruan, Y.Q. Yang, Mater. Sci. Eng. A 473 (2008) 274–278.
[25] W.H. Wang, Prog. Mater. Sci. 57 (2012) 487–656.
[26] W.H. Wang, J. Appl. Phys. 99 (2006), 1947-1358.
[27] R. Saha, Z.Y. Xue, Y. Huang, W.D. Nix, J. Mech. Phys. Solids 49 (2001) 1997–2014.
[28] R. Saha, W.D. Nix, Acta Mater. 50 (2002) 23–38.
[29] S. Chen, L. Liu, T. Wang, Surf. Coat. Technol. 191 (2005) 25–32.
[30] I.N. Sneddon, Int. J. Eng. Sci. 3 (1965) 47–57.
[31] T. Egami, Y. Waseda, J. Non-Cryst. Solids 64 (1984) 113–134.
[32] D. Pan, A. Inoue, D. Pan, A. Inoue, T. Sakurai, M.W. Chen, Proc. Natl. Acad. Sci. U. S. A. 105 (2008) 14769–14772.
[33] D. Pan, Y. Yokoyama, T. Fujita, Y.H. Liu, S. Kohara, A. Inoue, M.W. Chen, Appl. Phys. Lett. 95 (2009) 11–279.
[34] U.F. Kocks, H. Mecking, Prog. Mater. Sci. 48 (2003) 171–273.
[35] Y. Andersson, Chem. Scr. 28 (1988) 125–127.
[36] A. Nylund, J.Ø. Madsen, G. Schroll, J.H. Bowie, R. Records, Acta Chem. Scand. 20 (1966) 2381–2386.
[37] B. Aronsson, A. Nylund, S. Rundqvist, E. Varde, G. Westin, Acta Chem. Scand. 14 (1960) 1011–1018.
[38] J.J. Lewandowski, W.H. Wang, A.L. Greer, Philos. Mag. Lett. 85 (2005) 77–87.
[39] D. Ma, A.D. Stoica, X.L. Wang, Z.P. Lu, B. Clausen, D.W. Brown,Phys. Rev. Lett. 108 (2012), 085501.
[40] W. Zhao, G. Li, Y.Y. Wang, S.D. Feng, L. Qi, M.Z. Ma, R.P. Liu, Mater. Des. 65 (2015) 1048–1052.
[41] W. Zhao, J.L. Cheng, S.D. Feng, G. Li, R.P. Liu, Mater. Lett. 175 (2016) 227–230.
[42] Y.Q. Cheng, E. Ma, Prog. Mater. Sci. 56 (2011) 379–473.
[43] C. Dong, Z.J. Wang, S. Zhang, Y.M. Wang, Int. Mater. Rev. 65 (2019) 286–296.
[44] D.B. Miracle, Acta Mater. 54 (2006) 4317–4336.
[45] H.W. Sheng, W.K. Luo, F.M. Alamgir, J.M. Bai, E. Ma, Nature 439 (2006) 419–425.
[46] W.H. Wang, Nat. Mater. 11 (2012) 275–276.
[47] Z.F. Zhao, P. Wen, R.J. Wang, D.Q. Zhao, M.X. Pan, W.H. Wang, J. Mater. Res. 21 (2006) 369–374.